DAΦNE TECHNICAL NOTE

INFN - LNF, Accelerator Division

Frascati, May 22, 1997

Note: **MM-26**

THE DIPOLES OF THE DAΦNE MAIN RING ACHROMATS

B. Bolli, N. Ganlin, F. Iungo, F. Losciale, M. Paris,
M. Preger, C. Sanelli, F. Sardone, F. Sgamma, M. Troiani

1. Introduction

The measurements performed on the prototypes of the Main Rings achromats dipoles are described in [1,2]. In this Note we show the results of the systematic procedures followed to tune and measure each one of the 16 dipoles of the collider.

2. Data acquisition system

Figure 1 shows a block diagram of the acquisition system in its final configuration used to measure the series production dipoles of the DAΦNE Main Rings. It consists mainly of a Hall probe positioning system with 4 degrees of freedom Micro Controle mod. ITL09, with a resolution of 1 μ and an accuracy of ±10 μ. The ranges are 2.5 m for the X movement, 1.0 m for Y, 0.4 m for Z and 270° for the rotation of the Hall probe support. The positioning system is controlled by means of a MacIntosh Centris 650 equipped with a National NI488.2 plug for GP-IB connection with the surrounding equipment. The measurements are performed at a fixed temperature of 23 °C in the hall, obtained by means of an air conditioning system. All the probes have been calibrated at that temperature.

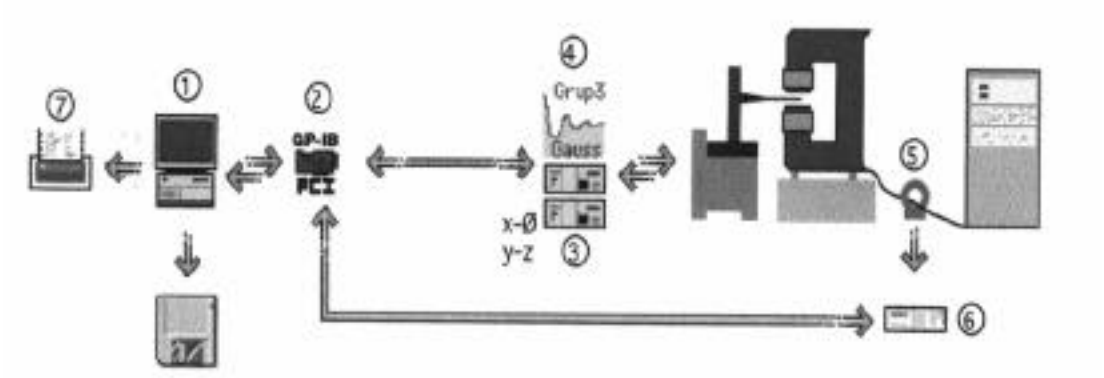

1 - MacIntosh Centris 650
2 - GP-IB board National NI-488.2
3 - MicroControle ITL09 positioning system
4 - Group3 Digital Hall Effect Teslameter
5 - Holec current transducer
6 - HP 3457A Multimeter
7 - HP Think Jet printer

Figure 1 - Block diagram of the data acquisition system.

The Group3 Digital Hall Effect Teslameter has a precision of ±0.01% on the reading ±0.006% of full scale. The current in the magnet is measured by means of a current transducer HOLEC 2250A/10V, with a linearity error of 5 ppm, a temperature sensitivity of 1 ppm of full scale/°K, and a long term stability of 1 ppm of full scale per month.

The acquisition program is written in LabVIEW 3.1 and collects the field measurements of one scan automatically. Few variables are the input to the program, namely the amplitude and the number of the steps in the straight part of the nominal trajectory, the step in the arc, the nominal bending radius of the magnet. Step by step, the program computes the X and Y coordinates to be transferred to the positioning system in order to drive the probe on the desired path. A software feedback loop controls the position of the probe, read from the encoders of the positioning system. The current in the magnet coil is controlled at each step, and the field measurement repeated if the current reading differs from the correct value by more than a pre-set value. At each step the program plots on the monitor screen the position of the probe and the measured field. The rate of the measurements is ≈10 points per minute. At the end of the scan the program creates a file where the X and Y positions of the probe, the longitudinal coordinate along the trajectory, the measured field and the measured current are recorded at each step. The magnetic length, calculated as the field integral divided by the maximum measured field in the scan is also shown on the monitor. Figure 2 shows the LabVIEW window of the control program.

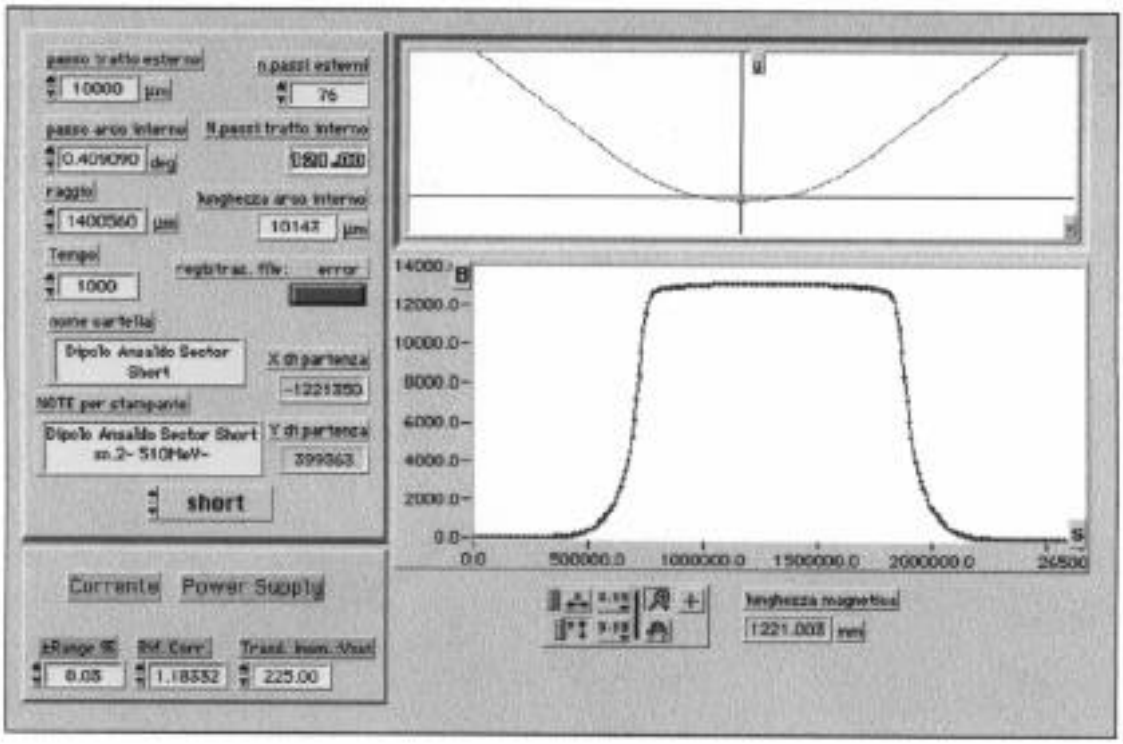

Figure 2 - LabVIEW window of the acquisition program.

3. Steel length optimization

Since all the dipoles in each ring are powered in series, the bending angle at the nominal current (266.2A) must be the same (49.5°) for all the long magnets in the outer arcs and a different one (40.5°), but the same for all the short magnets in the inner arcs. In order to obtain this result, a standard procedure has been followed for each dipole, in order to find the correct steel length. The correction range of the backleg coils at the nominal current and at few other operating points is discussed in [1,2].

The results of the measurements performed on the prototypes [1,2] have shown that the field integral along the real trajectory followed by the beam, and therefore the beam energy corresponding to the nominal bending angle, is a linear function of the total steel length. The magnets have been delivered with removable end caps, which can be properly machined to achieve the correct field integral, in spite of small construction differences between the dipoles.

For each magnet we have therefore measured a first field map with the original end caps consisting of one longitudinal scan along the nominal trajectory and 4 others along lines parallel to it at a distance of ±10 mm and ± 20 mm. A second order polynomial has been fitted to the 5 measured points at each azimuth on the nominal trajectory, in order to find the integrated second order term. The trajectory followed by the particles in the magnet has been calculated by means of a tracking code ("TRAJ" [3]), taking into account only the scan on the nominal trajectory and the two adjacent ones, since the maximum distance of the calculated trajectory from the nominal one never exceeds 6 mm. The condition that the final deflection be equal to the nominal bending angle determines the energy of the beam.

The same procedure (without the scans at ±20 mm) has been followed after removing the end caps (whose original thickness is ≈32 mm), and the corresponding beam energy for nominal deflection found. By interpolating linearly between these two energies, it is possible to find by which amount the end cap thickness must be reduced in order to find the same beam energy for all the dipoles. Starting from the first prototype (the Parallel Ends Short dipole [1]) this energy has been set at 511.8 MeV at an excitation current of 266.2A. A last map, consisting of 9 longitudinal scans up to ±40 mm, is performed after machining the end caps in order to find the final energy and the high order contributions up to the fourth power.

Table I shows the energies found for all the dipoles after the optimization procedure. Two iterations have been performed on PES#2 and SLS#4 before reaching the final configuration. The end caps of PEL#3 have been machined after the last map, reducing the thickness by 0.9 mm, without re-measuring the magnet. Its energy value in Table I is assumed (with a good level of confidence) to be the optimal one. Figure 3 is an histogram of the final energy distribution (obviously without any backleg winding correction).

Table I - Calculated beam energy for nominal deflection @ 266.2A

Dipole	**Cut depth (mm)**	**Energy (MeV)**
PES #1	20.00	511.824
PES #2	20.10	511.734
PES #3	20.20	511.855
PES #4	20.40	511.822
PEL #1	25.50	511.742
PEL #2	24.70	511.786
PEL #3	23.90	511.800
PEL #4	25.00	511.876
SLS #1	7.25	511.867
SLS #2	7.00	511.693
SLS #3	7.20	511.812
SLS #4	8.40	511.845
SLL #1	5.70	511.633
SLL #2	7.10	511.656
SLL #3	7.20	511.869
SLL #4	8.50	511.703

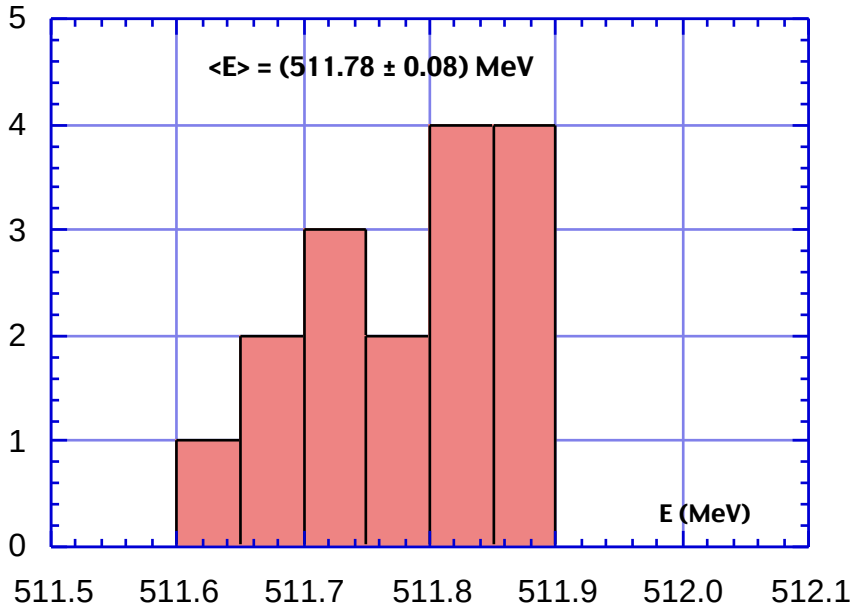

Figure 3 - Distribution of the final energy for nominal deflection @ 266.2A

4. Sextupole-like term minimization

As already described in [1,2,3], a shimming technique has been applied, in order to minimize the effects of the sextupole-like contribution to the chromaticity of the ring coming from a non-vanishing integrated second order term in the fringing field of the dipoles. Although this effect is smaller in the Main Rings dipoles than the result found for the Accumulator [3], we decided to keep the integrated second order term as small as possible.

The geometry shown in Figure 3.6 of Ref. [1] has been adopted for all the magnets, with the shim step starting at an horizontal distance of 70 mm from the original end cap outer face. It was found that the shim thickness, being the shim rather far (≥ 70 mm) from the pole center, does not affect the field integral, so that the optimization of the end cap thickness is independent from the optimization of the integrated second order term.

Table II shows the integrated second order term for all the dipoles, together with the height of the shim on the end caps. It can be observed that for the Parallel Ends dipoles, where the required reduction of the end cap thickness was found to be more than 20 mm, the shim heights are all the same (5.5 mm) for the long dipoles and almost the same (4.5 mm) for the short ones, with PES#3 having a slightly different value. For these magnets the correction of the second order term is better than the result obtained for the Sector-like magnets. The reason is that the Sector-like dipoles required a much smaller end cap reduction (see Table I), in most cases smaller than the optimum shim height for the sextupole-like term minimization. Due also to the strict tolerances on the outer size of the magnets, which must accurately match those of the vacuum chamber, it was decided not to mount additional shims on the end caps (as done in the case of the Accumulator dipoles [3]) and to accept the residual integrated second order contribution to the chromaticity of the rings.

The final situation is shown in Figure 4, where the light bars represent the Parallel Ends dipoles and the dark ones the Sector-like magnets. It can be observed that half of the dark bars tend to be clustered on the negative side of the distribution, corresponding to those magnets where the required shim height for a good correction of the sextupole-like contribution would have been larger than the cut performed on the end caps to reach the correct beam energy.

Table II - Integrated second order term of transverse fit
and shim height of the 16 dipoles

Dipole	Shim height (mm)	∫b2dl (T/m)
PES #1	4.5	-0.146
PES #2	4.5	-0.160
PES #3	5.0	0.037
PES #4	4.5	-0.159
PEL #1	5.5	-0.098
PEL #2	5.5	0.124
PEL #3	5.5	0.043
PEL #4	5.5	-0.041
SLS #1	8.0	-0.066
SLS #2	7.0	-0.063
SLS #3	7.2	-0.266
SLS #4	8.0	0.198
SLL #1	5.7	-0.307
SLL #2	7.1	-0.386
SLL #3	7.2	-0.286
SLL #4	8.5	-0.132

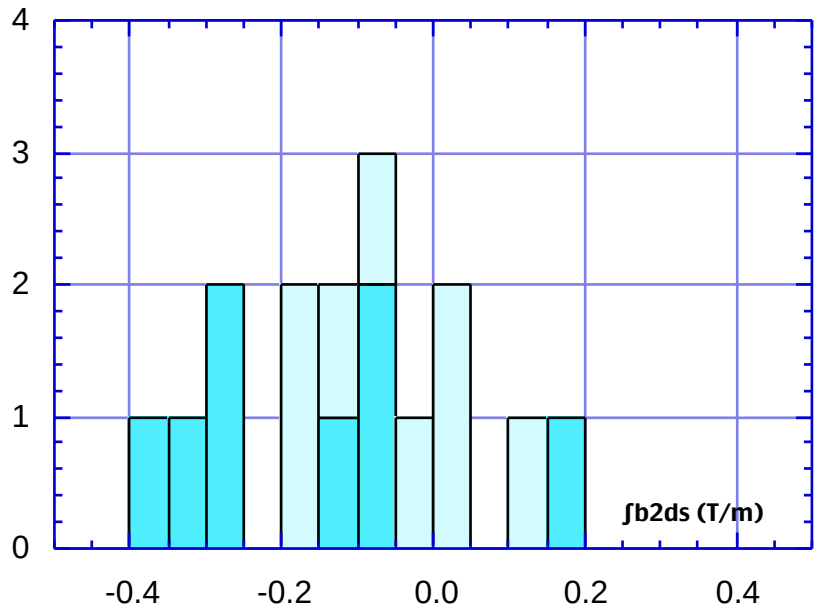

Figure 4 - Distribution of the integrated second order term of the transverse fit. (Light bars = Parallel Ends dipoles, dark bars = Sector-like dipoles).

5. Other high order terms in the transverse fit

As already mentioned in Section 3, a fourth order polynomial fit has been performed on all the dipoles as a function of the longitudinal position along the nominal trajectory, in the final configuration of end cap thickness and shim.

Table II gives the integrated first, third and fourth order contributions. As expected, the first order term is almost constant among the samples of the PES and PEL dipoles (the large value of the integrated term is due to the parallel ends geometry of the magnet). The small, but always positive, value for the Sector-like magnets, is due [1] to the fact that the iron yoke is shorter than the nominal length of the magnet while the angle between the end faces is the nominal one.

Table III - Integrated first, third and fourth order terms of transverse fit

Dipole	**∫b1ds (T)**	**∫b3ds (T/m^2)**	**∫b4ds (T/m^3)**
PES #1	-0.771	6.059	-22.237
PES #2	-0.764	5.972	-41.087
PES #3	-0.765	6.370	-52.069
PES #4	-0.766	6.041	-12.865
PEL #1	-0.954	9.958	-39.380
PEL #2	-0.953	8.514	-64.341
PEL #3	-0.954	8.428	-65.295
PEL #4	-0.958	8.589	-31.858
SLS #1	0.026	0.623	39.155
SLS #2	0.016	-0.293	-13.727
SLS #3	0.018	-1.141	-11.410
SLS #4	0.019	-2.103	-72.659
SLL #1	0.010	-0.546	-47.608
SLL #2	0.011	-1.363	50.924
SLL #3	0.010	-1.465	12.030
SLL #4	0.012	-1.500	17.970

Figure 5 shows the distribution of the third order term: as expected, the contribution for the Sector-like dipoles is smaller than for the Parallel Ends ones, since the third order contribution comes mainly from the distortion of the linear term.

The integrated fourth order term distribution is given in Figure 6. It should be remarked that both the integrated third order term (for the Sector-like dipoles) and the fourth order one are about one order of magnitude smaller than those found for the Accumulator dipoles [3].

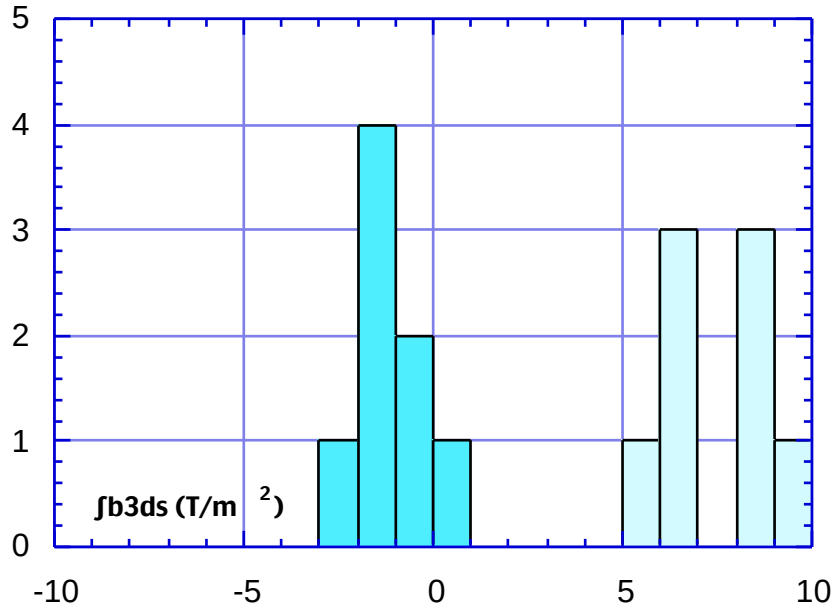

Figure 5 - Distribution of the integrated third order term of the transverse fit. (Light bars = Parallel Ends dipoles, dark bars = Sector-like dipoles)

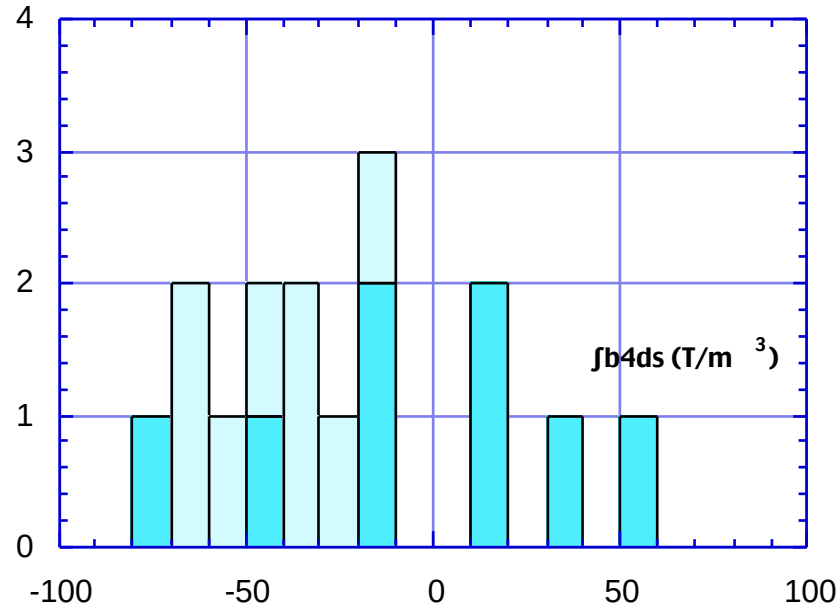

Figure 6 - Distribution of the integrated fourth order term of the transverse fit. (Light bars = Parallel Ends dipoles, dark bars = Sector-like dipoles)

6. Orbit-related parameters

As mentioned in Section 3, the trajectory followed by the particles inside the magnet has been calculated for each dipole by means of a tracking program which interpolates between the measured field values. An example of such trajectories for the short dipoles is shown in Figure 3.7 in Ref. [1] and for the long ones in Fig. 3.6 in Ref. [2]. The most interesting parameters of these trajectories are the maximum distance ΔX from the nominal trajectory, the shortening ΔL of the calculated orbit with respect to the nominal one and the offset δX of the calculated trajectory at the output of the magnet due to asymmetries of the field with respect to the geometric symmetry axis of the dipole. These parameters are summarized in Table IV for the 16 dipoles.

An important consequence of the orbit shortening in the dipoles is the shift in the revolution frequency of the rings, which can be calculated from Table IV. The positron ring is 16.49 mm shorter than its nominal value. The shortening for the electron ring is 16.37 mm. The corresponding shift in the RF frequency (120th harmonic of the revolution) is $\approx$ 62 KHz.

Figure 7 shows the distribution of the maximum distance between the calculated and nominal trajectories. The negative sign of the displacement indicates that the particle orbit lies on the inner side of the nominal trajectory. The effect is clearly larger for the Sector-like dipoles and this reflects on the shortening of the trajectory, given in Figure 8, where, however, the average value for the Sector-like short dipoles is similar to the corresponding one for the Parallel Ends long ones.

Figure 9 shows the offset of the trajectory at the output of the dipole, under the assumption that the particles enter the magnets on the nominal trajectory. A positive value for the offset indicates that the trajectory at the output is on the outer side of the ring.

Table IV - Orbit related parameters for the 16 dipoles

Dipole	**ΔX (mm)**	**ΔL (mm)**	**δX (mm)**
PES #1 (e^-)	-2.55	-1.67	-0.25
PES #2 (e^+)	-2.58	-1.74	0.02
PES #3 (e^+)	-2.80	-1.88	-0.22
PES #4 (e^-)	-2.55	-1.69	0.15
PEL #1 (e^-)	-2.48	-1.81	0.18
PEL #2 (e^+)	-2.48	-1.94	0.00
PEL #3 (e^+)	-2.52	-1.99	0.00
PEL #4 (e^-)	-2.53	-1.92	0.02
SLS #1 (e^+)	-3.30	-1.97	0.19
SLS #2 (e^-)	-3.35	-2.02	0.08
SLS #3 (e^-)	-3.28	-1.97	0.22
SLS #4 (e^+)	-3.25	-1.97	0.04
SLL #1 (e^-)	-3.63	-2.67	0.07
SLL #2 (e^+)	-3.38	-2.51	0.09
SLL #3 (e^-)	-3.52	-2.62	0.02
SLL #4 (e^+)	-3.31	-2.49	0.05

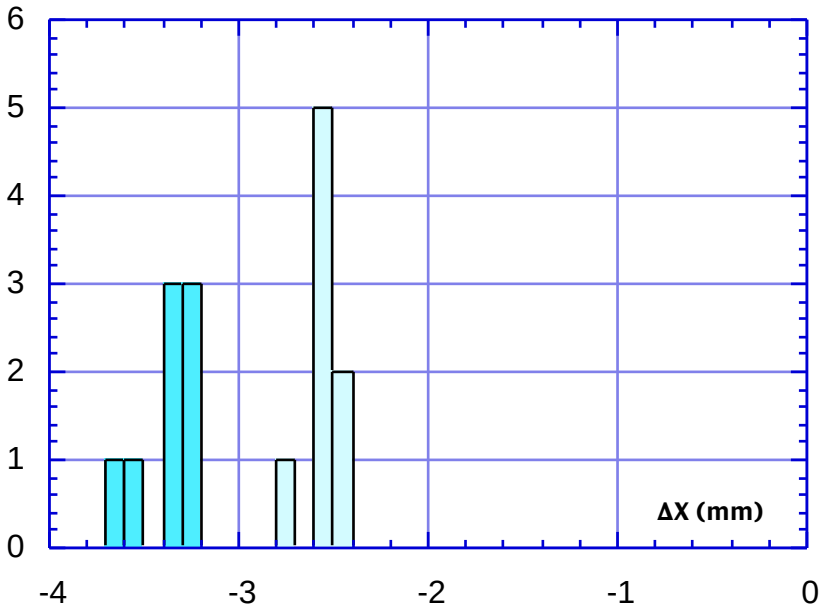

Figure 7 - Distribution of the maximum distance between the calculated and nominal trajectories. (Light bars = Parallel Ends dipoles, dark bars = Sector-like dipoles)

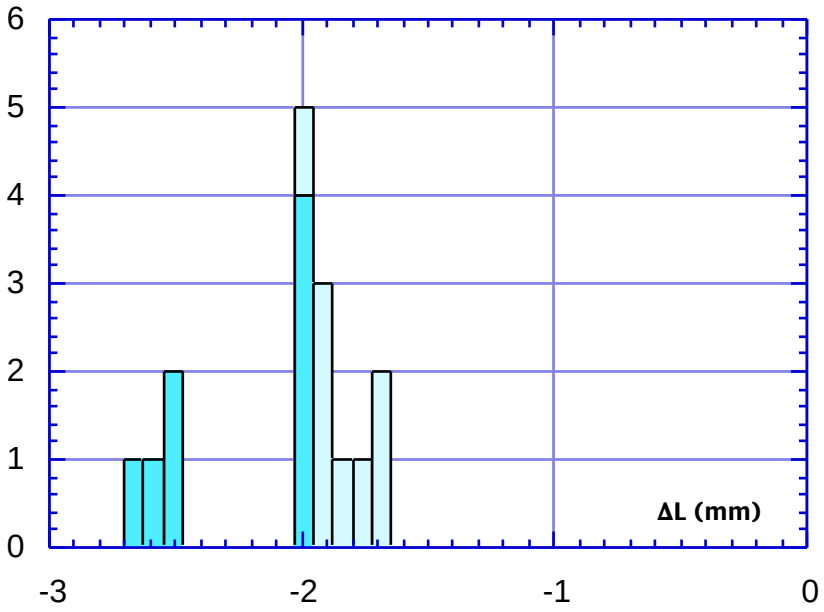

Figure 8 - Distribution of the orbit shortening in each dipole. (Light bars = Parallel Ends dipoles, dark bars = Sector-like dipoles)

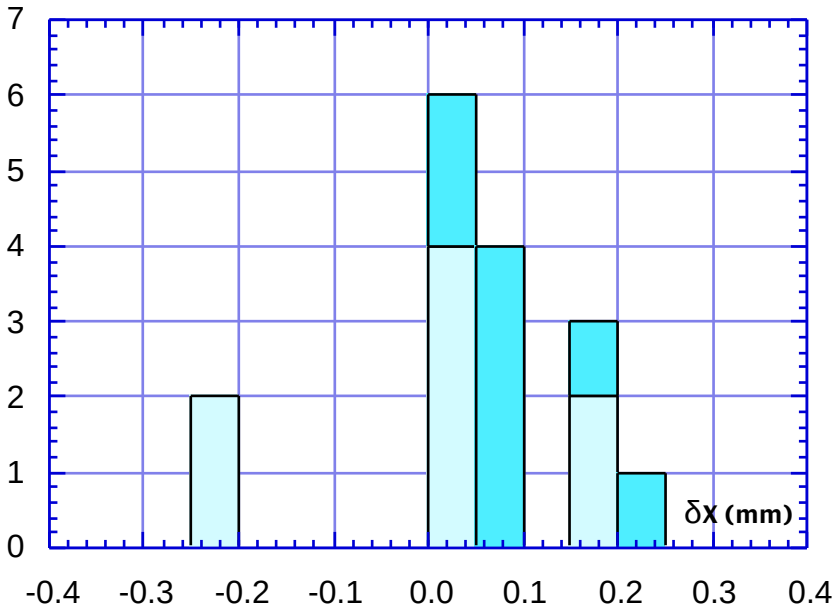

Figure 9 - Distribution of the offset at the output of the dipoles.
(Light bars = Parallel Ends dipoles, dark bars = Sector-like dipoles)

References

[1] B. Bolli, N. Ganlin, F. Iungo, F. Losciale, M. Modena, M. Paris, M. Preger, C. Sanelli, F. Sardone, F. Sgamma, M. Troiani "The "short" dipoles of the DAΦNE Main Ring achromats" - DAΦNE Technical Note MM-19 (2/8/1996).

[2] B. Bolli, N. Ganlin, F. Iungo, F. Losciale, M. Paris, M. Preger, C. Sanelli, F. Sardone, F. Sgamma, M. Troiani "The "long" dipole prototypes of the DAΦNE Main Ring achromats" - DAΦNE Technical Note MM-25 (21/5/1997).

[3] A. Battisti, B. Bolli, F. Iungo, F. Losciale, M. Paris, M. Preger, C. Sanelli, F. Sardone, F. Sgamma, M. Troiani, S. Vescovi "Measurements and tuning of DAΦNE Accumulator dipoles" - DAΦNE Technical Note MM-9 (29/8/1995).